Structural and magnetic properties of Co_xSi_{1-x} thin films and multilayers

2007 J. Phys.: Condens. Matter 19 486003

(http://iopscience.iop.org/0953-8984/19/48/486003)

IOP PUBLISHING JOURNAL OF PHYSICS: CONDENSED MATTER

J. Phys.: Condens. Matter **19** (2007) 486003 (14pp) doi:10.1088/0953-8984/19/48/486003

Structural and magnetic properties of Co_xSi_{1-x} thin films and multilayers

C Quirós[1], L Zárate[1], J Díaz[1], P Prieto[2], J Rubio-Zuazo[3] and J M Alameda[1]

[1] Departamento de Física, Universidad de Oviedo, Avenida Calvo Sotelo, s/n, E-33007 Oviedo, Spain
[2] Departamento de Física Aplicada, C-XII, Universidad Autónoma de Madrid, E-28029 Cantoblanco, Spain
[3] SpLine, Spanish CRG BM25 Beamline, ESRF, BP 220, F-38043 Grenoble, France

Received 18 May 2007, in final form 5 September 2007
Published 9 November 2007
Online at stacks.iop.org/JPhysCM/19/486003

Abstract

The structural and magnetic properties of thin films and multilayers based on Co_xSi_{1-x} magnetic layers and Si spacers have been studied by surface x-ray diffraction, Auger electron spectroscopy and magneto-optical transverse Kerr effect measurements. Surface x-ray diffraction has been used to follow the evolution of the Co lattice as Si is incorporated into the network for the low Si content range, $1.00 \leqslant x \leqslant 0.77$, and a contraction of the unit cell, around 0.2% out-of-plane and 0.9% in-plane, has been found. No fingerprint of structural anisotropy in the grain size, either parallel or perpendicular to the magnetic easy axis, has been detected. Magneto-optical transverse Kerr effect hysteresis loops of single films show both an increase of coercive field and a rotation of the magnetic anisotropy axis as Si enters the lattice in the polycrystalline range, $1.00 \leqslant x \leqslant 0.85$. For the multilayer case, the loops confirm the formation of antiferromagnetic ordering through the layers when the composition of the alloy is tuned to be in the amorphous range. The corresponding AES signals show asymmetric depth profiles, suggesting the formation of intermediate compounds at the broader Co-on-Si interfaces.

(Some figures in this article are in colour only in the electronic version)

1. Introduction

Interlayer exchange coupling through semiconducting spacers has attracted strong attention in recent years, the Fe–Si system being the most intensively studied [1–7] although, recently, several works have also focused on the Co–Si system. In particular, amorphous Co_xSi_{1-x} alloys separated by Si spacers have been shown to couple antiferromagnetically with very low switching fields, of the order of a few Oe [8, 9]. Also, polycrystalline pure Co/Si multilayers have been shown to develop superparamagnetic, ferromagnetic [10], antiferromagnetic [11] or oscillatory [12, 13] behaviours. In many cases diffusion processes have been reported and their

influence on the magnetic coupling seems to be relevant [3, 14]. All this experimental work has also stimulated several theoretical approaches concerning the origin of the coupling through semiconducting spacers [15–17].

In order to improve the comprehension of the magnetic and structural properties of these multilayered systems, good understanding of the basic properties of the corresponding single thin films is required. Some facts already well established about Co_xSi_{1-x} single films are the presence of an amorphous/polycrystalline transition at around $x = 0.75$ and the softer magnetic behaviour of the amorphous films. Detailed works by Fallon *et al* [18, 19], have studied the evolution of the structure with the Si content, although their deposition conditions are very different from the ones used in this work, since their films were grown at higher pressures and higher growth rates. More recent works have carefully characterized the evolution of magnetic anisotropy and coercive field as the composition of Co–Si films is varied through the polycrystalline/amorphous transition, confirming the softer and more anisotropic behaviour of the amorphous films [20, 21]. However, although the origin of this magnetic anisotropy is, in principle, related to the oblique incidence of Si atoms during growth, the structural details leading to it are yet to be understood. In relation to this open question, extended x-ray absorption fine structure (EXAFS) measurements suggest that Si induces the formation of an amorphous phase in the polycrystalline matrix, and a reduction of the first neighbours interatomic distance has been found [21].

Recent works have studied the growth of ordered cobalt silicides in Co films grown on top of Si substrates or in Co/Si multilayers. In particular, cobalt silicide formation has been shown to depend on the Si terrace size, on the annealing temperatures and on the relative Co/Si thicknesses [22–29]. However, other works show no clear evidence of cobalt silicide formation at Co/Si interfaces at room temperature and indicate a dependence of the Co texture on the Si layer thickness [30]. Finally, it is worth mentioning that ordered nanodots of cobalt silicide have been prepared by using polystyrene nanospheres lithography, with sizes and shapes that can be controlled by adjusting the lithography and annealing conditions [31].

In this context, the main purposes of the present work can be summarized in the following three points and the corresponding results are discussed in section 3.

(a) Characterization, by surface diffraction techniques, of the structural changes induced in the crystalline network of Co_xSi_{1-x} films as the Si content is increased and the amorphization proceeds, focusing on the polycrystalline range where diffraction measurements can give valuable information. Special attention has been paid to the changes observed both in the in-plane and out-of-plane diffraction peak positions and widths, related to variations in the unit cell size and grain size, respectively.
(b) Study of the evolution of the corresponding magnetic hysteresis loops, following the behaviour of the magnetic anisotropy and coercive field with Si content and comparing it with the crystalline structural features. Specific measurements have been carried out to check if there are differences in the grain size along both magnetically relevant directions of the films that could be affecting the magnetic anisotropy.
(c) Characterization of the interface structure, stacking sequence and magnetic behaviour of Co_xSi_{1-x}/Si multilayers, which, as already mentioned, have been shown to develop antiferromagnetic coupling for compositions in the amorphous range [8, 9].

2. Experimental details

Samples have been prepared at room temperature by co-sputtering of pure Co and pure Si 2 inch diameter targets in a system with 10^{-9} mbar base pressure. During deposition, Ar pressure was

fixed at 1.0×10^{-3} mbar and the growth rates have been kept in the range 0.7–1.2 Å s^{-1}. Both targets are mounted on two flanges which lie in the vertical plane, while the substrate normal lies in the horizontal plane. The Co target is in front of the substrate, whereas Si is 30° off the substrate normal. This is an important detail since the magnetic anisotropy observed in these films is related to the balance between normal incidence Co atoms and oblique incidence Si ones.

Two types of substrates have been used: Si(111) wafers with native oxide on top and amorphous fused silica substrates. In both cases the shape of the substrates was rectangular, typical size around 10 mm × 8 mm, and the long side was kept horizontal during growth in order to have a reference to evaluate the effect of oblique Si incidence. Amorphous fused silica substrates have been used to reduce spurious contributions to diffraction patterns coming from the crystalline substrate background.

Two different sets of samples have been prepared with different compositions: (a) Co_xSi_{1-x} films; (b) Co_xSi_{1-x}/Si multilayers. In all cases a Si capping has been grown on top to prevent oxidation, and a Si buffer has been initially grown on the substrate so that the magnetic layer growth starts always from fresh Si. The capping and buffer thickness have been fixed at 3 nm for the case of single films and are equal to the Si spacer thickness for the case of multilayers (so that the multilayer symmetry is preserved).

Magnetic properties have been studied by the magneto-optical transverse Kerr effect (MOTKE) [32]. The Kerr signal has been defined, as usual in the transverse configuration, as the change in reflectivity induced by the magnetic state divided by the average reflectivity of the sample. Auger electron spectroscopy (AES) composition depth profiles have been performed with 3 KeV Ar^+ ions in a Phi 3027 spectrometer equipped with a double pass cylindrical mirror analyser (10^{-10} Torr base pressure). AES signals have been corrected by the corresponding sensitivity factors of each element. Structural information has been obtained by x-ray diffraction measurements. Two systems have been used, a laboratory Phillips X'PERT PRO diffractometer, using Cu Kα radiation, and also the six circle vertical axis diffractometer of beamline BM25 (Spline) at the European synchrotron radiation facility (ESRF), using 19.72 keV photons. The diffraction patterns obtained in the six circle diffractometer have been denoted with the usual surface x-ray diffraction (SXRD) convention, that is, the reciprocal lattice axis H and the K axis are lying in the film plane and the L axis is perpendicular to the film surface. The real space lattice basis vectors have been chosen to match the Co FCC structure, with moduli $a_1 = a_2 = 2.507$ Å (first neighbour distance) and $a_3 = 6.140$ Å (three times the interplanar distance 2.047 Å) and having angles between them of $\alpha_1 = \alpha_2 = 90°$, $\alpha_3 = 120°$. The corresponding reciprocal basis vectors are: $a_1^* = a_2^* = 2.895$ $Å^{-1}$ (parallel to the H and K axes, respectively) and $a_3^* = 1.023$ $Å^{-1}$ (parallel to the L axis) with angles $\alpha_1^* = \alpha_2^* = 90°$, $\alpha_3^* = 60°$. In-plane and non-specular out-of-plane scans have been acquired at grazing incidence, 2°, in order to enhance the thin film signal with respect to the substrate background.

3. Results and discussion

In the following sections the results obtained for the two sets of samples, single films or multilayers, are presented and discussed.

3.1. Polycrystalline Co_xSi_{1-x} films

The research has focused on low Si content samples, which have been less studied in previous works. Apart from a pure Co reference sample, $x = 1.00$, three more films have been prepared,

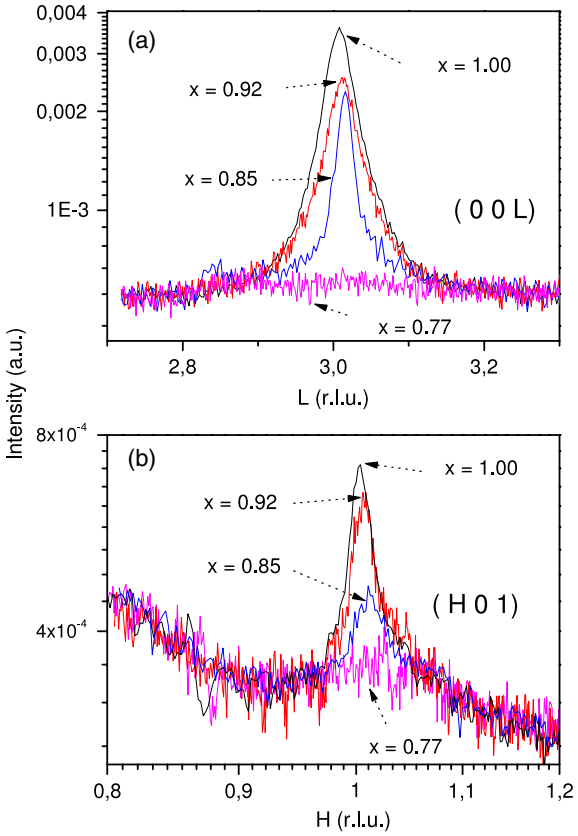

Figure 1. (a) (0 0 L) scans of 50 nm thick Co_xSi_{1-x} films with x in the range 1.00–0.77; (b) (H 0 1) scans of 50 nm thick Co_xSi_{1-x} films with x in the range 1.00–0.77. Peaks are on a decreasing background going from left to right.

corresponding to Co atomic fractions of $x = 0.92$, 0.85 and 0.77. All of them are 50 nm thick and have been grown on amorphous fused silica substrates with a 3 nm Si buffer and a 3 nm Si capping. In order to follow the modifications induced by the Si on the lattice parameters and grain size induced, two types of scans mapping the reciprocal space have been acquired: (00L) scans, to follow out-of-plane stacking, and (H 0 1) scans, to monitor in-plane ordering.

Figure 1(a) shows the evolution of the (0 0 3) specular peak when Si concentration is increased. The trend shows that the position of the peak shifts to higher values in reciprocal space, meaning that the interplanar distance perpendicular to the film plane decreases when Si atoms enter the network. The reduction of peak intensity suggests that the amorphization process is continuously taking place as Si is introduced in the network.

When the reciprocal space is mapped around the H direction in the (H 0 1) scans, figure 1(b), information of in-plane ordering is obtained. Again, following the same trend observed in the specular scans, the Si incorporation to the lattice leads to a shift of the (1 0 1) peak towards higher values in reciprocal space, now meaning that the in-plane lattice parameter also decreases with Si content. This behaviour may be related to the smaller atomic size of Si as compared to Co. The trend is similar both for the in-plane and out-of-plane directions, as can be visualized in figure 2(a). It indicates a unit cell contraction of around 0.9% in-plane and 0.2% out-of-plane with respect to the pure Co unit cell. This result agrees with previous reports from

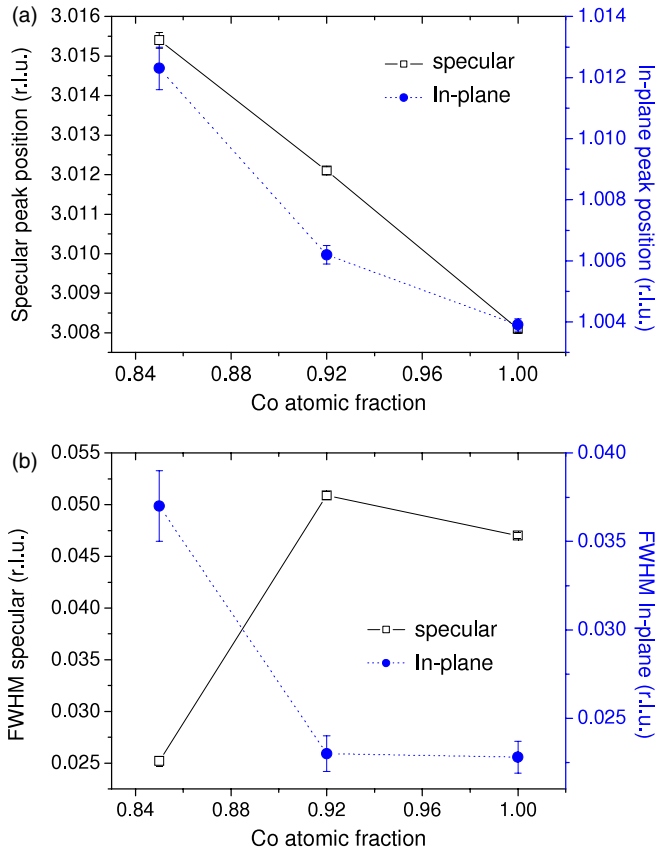

Figure 2. (a) Position of the (0 0 3) peak, in specular scans (open squares), and the (1 0 1) peak, in in-plane scans (filled circles), peaks as a function of Co concentration; (b) corresponding FWHM of the same peaks. Continuous and dotted lines are shown just as a guide to the eye. Error bars have been obtained from the fits.

EXAFS measurements, in the amorphous range, where the first shell radius has been found to decrease when increasing Si concentration in Co–Si polycrystalline films [21]. On the other hand, the evolution of FWHM for both peaks, shown in figure 2(b), suggests a sequence in which the incorporation of Si into the network does not produce significant changes either for the in-plane or out-of-plane grain sizes in the compositional range $0.92 \leqslant x \leqslant 1.00$. However, when the Si content is increased up to $x = 0.85$, the acceleration of the amorphization process, again indicated by the reduction of the peak area, is accompanied by clear changes in the grain size, leading to the growth of crystallites that are smaller in the film plane dimension and larger in the out-of-plane direction. Finally, the film with higher Si content, $x = 0.77$, still shows some degree of crystallinity, but the corresponding peak position and FWHM values have not been included in figure 2 since the peaks are so weak and broad that no reliable estimation can be obtained. In any case, the grains further reduce in size, both in-plane and out-of-plane, as the amorphous/polycrystalline threshold is approached.

It is worth mentioning that the peak positions and FWHM shown in figure 2 have been estimated after fitting the corresponding peaks of figure 1 with Lorentzian shape curves. For the case of the specular peaks, just one component was enough to obtain good quality fits,

whereas two components have been used for the case of the in-plane peaks. The data shown in figure 2 for the in-plane peak position and FWHM correspond to the strongest of these two components, the one having ∼80% of the total peak area and centred around $H = 1.008$. The other contribution, ∼20% of the total peak area for the three compositions, has been used to account for the shoulder observed at around $H = 1.060$. The corresponding fits of the in-plane peaks, showing the two components used and the experimental data after linear background correction from $H = 0.9$ to 1.2, are shown in figure 3. Interestingly, the width of the weakest contribution is continuously decreasing as the Si content is increased, whereas its relative area increases, from 20.5% to 22.7% of the total peak area, for the $1.00 \leqslant x \leqslant 0.85$ range. This behaviour suggests that this component may be related to grains that are more stable during the amorphization process than the ones related to the stronger component.

In addition to the (0 0 L) and (H 0 1) scans, and taking advantage of the six circle diffractometer geometry, a non-specular (1 0 L) scan has been acquired for the pure Co film. This scan has the advantage of being able to distinguish ABCABC... stacking from fcc structure from the ABABAB... stacking characteristic of hcp ordering [33]. In the first case, two peaks are expected at around $L = 1$ and 2 (one for ABCABC . . . and the other for the ACBACB . . .). For the hcp case a peak should appear at around $L = 1.5$ [34]. The (1 0 L) scan depicted in figure 4 shows a clear peak at around $L = 1$, a second peak, less intense, around $L = 2$ and no peak in the middle. This means that the predominant stacking corresponds to fcc type, although the strong background suggests that smaller fractions of disordered and/or hcp stacking may also be present in the film. A further step can be given to check the in-plane mosaicity by sitting on top of the (1 0 1) peak and rocking the sample around the azimuthal axis normal to the surface. The result, not shown, is a flat scan with no significant intensity changes, meaning that the mosaicity is homogeneous, with no preferential in-plane ordering.

Concerning the magnetic characterization of these films, the corresponding MOTKE loops are shown in figure 5 for the samples discussed above. Also, a 50 nm thick amorphous sample, $x = 0.74$, grown on Si(111) with native oxide, has been included as a reference. As already mentioned, the substrates have rectangular shape and their long side has been kept during growth perpendicular to the evaporation plane (EP). In the geometry used, this plane, defined by the two target and the substrate normals, is the vertical plane. The magnetic field for measuring the loops has been applied, along the sample surface, either parallel to the evaporation plane (i.e. parallel to the substrate short side) or perpendicular to it (i.e. parallel to the substrate long side). The loops show that all the films have a certain degree of magnetic anisotropy, in principle related to the Si oblique incidence, but only the amorphous one, $x = 0.74$, has a well-defined easy axis, which is oriented along the substrate long side, that is, perpendicular to the evaporation plane. Interestingly, as can be seen in figure 5, the direction of the magnetic easy axis is the same for $x = 1.00$, 0.77 and 0.74 films, that is, perpendicular to the evaporation plane, but it rotates 90° for the intermediate polycrystalline compositions, $x = 0.92$ and 0.85, where the easy axis is parallel to the evaporation plane.

In order to verify if some structural anisotropy is playing a key role in the evolution of magnetic anisotropy observed in figure 5, two in-plane (H 0 1) scans have been measured for each sample: one defining the H reciprocal lattice axis to be parallel to the sample long side (i.e. perpendicular to the evaporation plane) and the other redefining H to be parallel to the sample short side (i.e. parallel to the evaporation plane). The result is shown in figure 6 for the four compositions. All the scans have a peak around $H = 1$ whose position is related to the lattice parameter and whose width is linked to the grain size. Figure 6 shows that, for all the samples, both (H 0 1) scans are identical when they are measured corresponding to the H axis parallel or perpendicular to the evaporation plane. This means that no significant differences are observed in the lattice parameter or in the grain size of

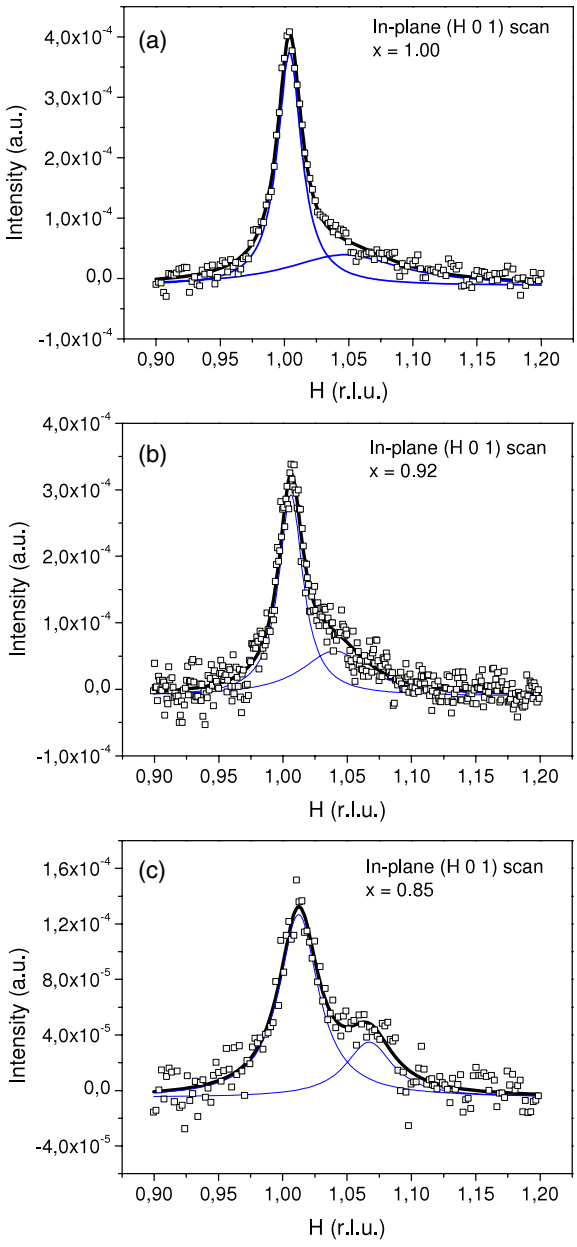

Figure 3. Lorentzian components (thin lines) used to fit the experimental data (open symbols), after linear background correction, for (a) $x = 1.00$, (b) $x = 0.92$ and (c) $x = 0.85$. The corresponding fits are shown as a thick line.

the crystals along both magnetically relevant directions of the sample. It is also worth considering the relative evolution of both components observed in the in-plane SXRD peaks (cf figure 3) and of the arrangement of the incipient amorphous areas formed as Si concentration increases. The competition between the magnetic contribution from these polycrystalline and amorphous areas may lead to the observed rotation of the magnetic easy axis direction for the

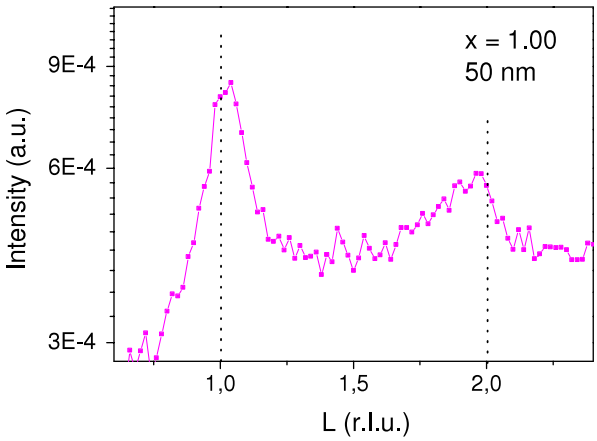

Figure 4. Non-specular (1 0 L) scan of 50 nm thick Co film. Dotted lines mark the position corresponding to $L = 1$ and 2.

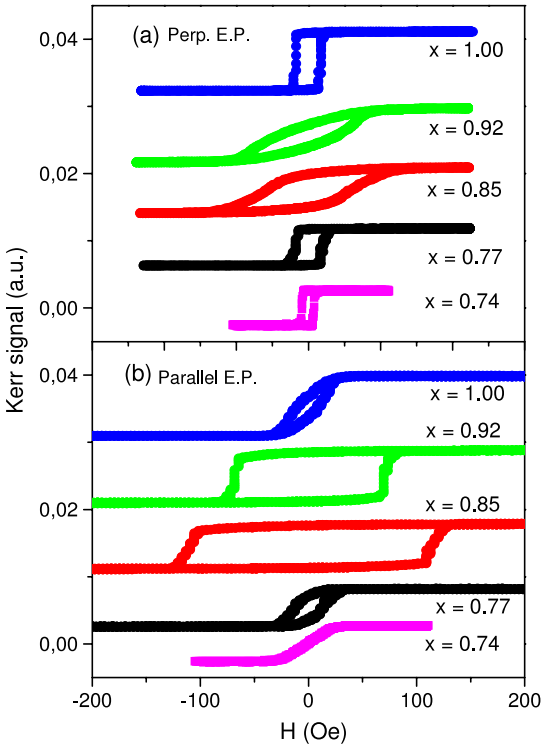

Figure 5. (a) MOTKE loops for magnetic field applied perpendicular to the evaporation plane; (b) MOTKE loops for magnetic field applied parallel to the evaporation plane.

samples having $x = 0.92$ and 0.85, although more information is needed to elucidate this point.

Another remarkable fact shown in figure 5 is the strong increase of the coercive field as Si atoms are incorporated into the film, having a maximum at $x = 0.85$. One aspect to consider

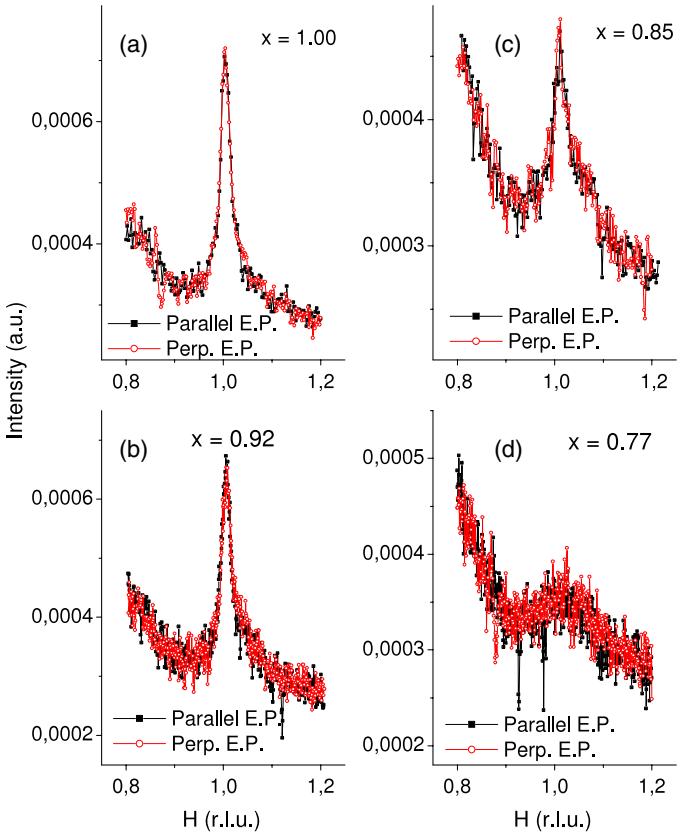

Figure 6. In-plane (H 0 1) scans measured for the four 50 nm thick samples with $x = 1.00$, 0.92, 0.85 and 0.77. In each panel two scans are shown, one for the H axis oriented parallel to the evaporation plane and the other redefining the H direction to be perpendicular to the evaporation plane.

in order to understand this behaviour is the reduction of the total magnetization as Si enters the lattice. Also, the increase of FWHM of the in-plane peak corresponding to $x = 0.85$, shows that in-plane grain size is being reduced, so that the density of grain junctions that can act as domain wall pinning centres increases, giving an additional contribution to the increase of coercive field. However, more subtle details should be taken into account since the increase in coercive field is already observed for Co rich concentrations, like $x = 0.92$, where the grain size is quite similar to the one of the pure Co film. In particular, the Si induced defect distribution may play an increasingly relevant role from the very beginning of the amorphization process, even when the grain sizes have not significantly changed, offering extra domain wall pinning centres. Again, the arrangement and size of the incipient amorphous areas may also affect the pinning of the domain walls. Finally, when the composition is further reduced to $x = 0.77$, although some degree of crystallinity still exists, the disordered amorphous regions may become dominant, so that fewer domain wall pinning centres exist and the film becomes softer. Also the magnetic anisotropy comes back to the orientation characteristic of the amorphous compositional range. However, uniaxial magnetic anisotropy with closed hard axis loops is only obtained when the amorphization process is completed, since, in that case, there are no crystals randomly oriented and the local anisotropy is not spread around several directions.

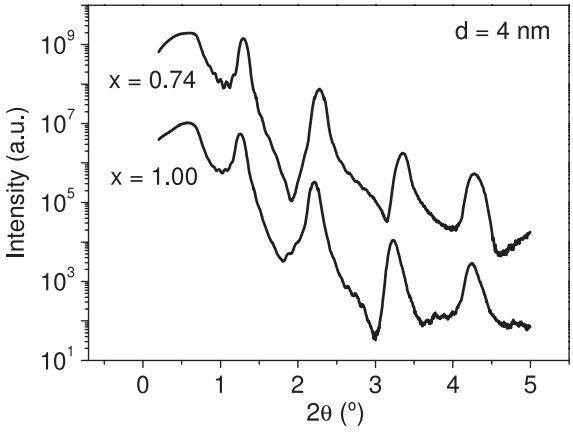

Figure 7. Low angle reflectivity patterns of 10 period multilayers. Each period is made of 5 nm magnetic material and 4 nm Si spacer. One multilayer has been made with magnetic layers having $x = 0.74$ and the other with $x = 1.00$.

3.2. Co_xSi_{1-x}/Si multilayers

From the above discussion it is evident that the composition of Co_xSi_{1-x} thin films has a clear influence on their structural and magnetic properties. As a result, the magnetic behaviour and structure of Co_xSi_{1-x}/Si multilayers is also expected to be strongly dependent on their composition. In order to study this dependence, several multilayers have been prepared with the following structure: $(Si^d/Co_xSi^{5\ nm}_{1-x})_n/Si^d$/substrate, where d is the Si layer thickness in nm (4–15 nm) and n is the number of periods of the multilayer ($n = 6$ for multilayers having $d = 15$ nm and $n = 10$ for multilayers with $d = 4$ nm). The magnetic layer thickness has been kept fixed at 5 nm. Two compositions have been chosen, one corresponding to the amorphous range, $x = 0.74$, and the other to the polycrystalline one, $x = 1.00$.

As a first characterization, grazing incidence x-ray reflectivity curves, using Cu Kα radiation, have been measured in order to verify if the stacking of both multilayers is well defined. The corresponding curves are shown in figure 7 for the case $d = 4$ nm, where the first four orders corresponding to the multilayer periodicity are clearly observed, meaning that the multilayer structure is well preserved after growth. These periodicities correspond to distances of ∼9 nm, which fits the nominal periodicity of 5 nm + 4 nm, corresponding to the nominal thickness of the magnetic layer + Si spacer. In addition to the different orders related to the multilayer periodicity, some oscillations related to the total sample thickness are also visible.

It is worth noting that previous analyses of reflectivity curves, measured in this kind of multilayers for the case of 2 nm thick Si spacers, suggest the formation of asymmetries at the interfaces, pointing to the growth of intermediate $CoSi_y$ compounds in the Co-on-Si interface, whereas the Si-on-Co interface appears with a sharper profile [8]. This trend, indirectly derived from the analysis of XRD reflectivities, has now also been observed by AES depth profiling, as can be seen in figure 8, panel (a) for the case $x = 0.74$ and panel (b) for $x = 1.00$. For carrying out these depth profiles, and in order to make easier the characterization of each interface, two multilayers having a thicker Si spacer, $d = 15$ nm, have been prepared so that the AES measurements are able to distinguish between different layers. AES profiles monitoring Co LMM, Si KLL, C KLL and O KLL peaks confirm again that the periodicity of both multilayers is well defined, with periodic changes in both Co and Si signals arising from the stacking sequence of the multilayer, as expected from the observation of multilayer

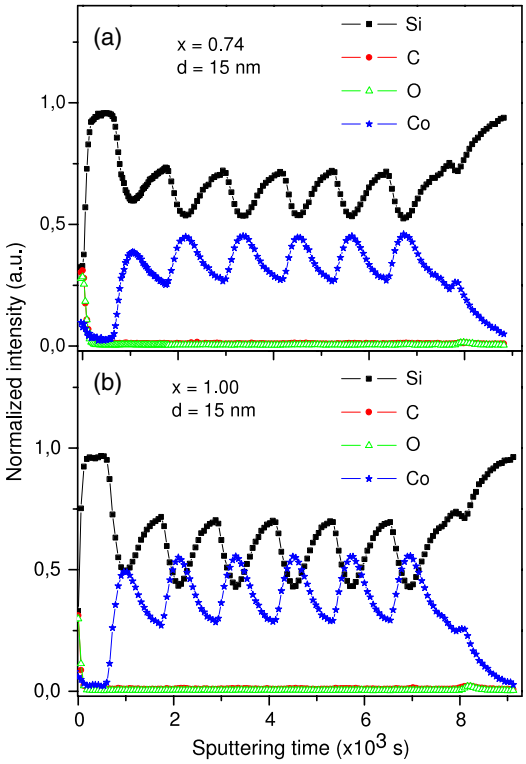

Figure 8. AES depth profiles of Co LMM, Si KLL, C KLL and O KLL signals of six period multilayers with a 15 nm Si spacer; (a) 5 nm amorphous magnetic layers ($x = 0.74$); (b) 5 nm polycrystalline magnetic layers ($x = 1.00$).

peaks in the XRD reflectivity patterns. The compositional profiles also show that the samples have a low contamination level, since, apart from the usual C and O surface contamination, also slightly observed in the sample/substrate interface, the C and O signals inside the layers remain always negligible. The layers are resolved in both samples, although they appear convoluted with mixing processes induced by the 3 keV Ar^+ ions used to carry out the profile that avoid the Co signal to go completely down to zero in the Si layers and vice versa. The Co/Si signal ratio in the Co layer is higher for the nominally 100% Co sample, as it should be. However, the most relevant feature observed in the AES profile is the asymmetric saw tooth like shape of the Si and Co peaks. The asymmetry shows that the width of the Co-on-Si interface is higher than the Si-on-Co one (a factor 1.8 higher). This feature is compatible with the formation of a $CoSi_y$ intermediate compound at the broader interface, as already suggested by XRD analysis [8], although possible asymmetric mixing effects should also be taken into account. It is worth mentioning that interface compounds and asymmetries resembling the ones discussed above have also been reported in other multilayered systems [35, 36]. The formation of such intermediate compounds is related to the activation of diffusion processes at the interfaces [19, 37].

Finally, concerning the magnetic properties of these multilayers it is worth recalling the strong compositional dependence of the single film magnetic behaviour. As previously discussed, the main structural difference between both compositions is that for $x = 0.74$ the magnetic material has an amorphous arrangement, whereas the case $x = 1.00$ leads to

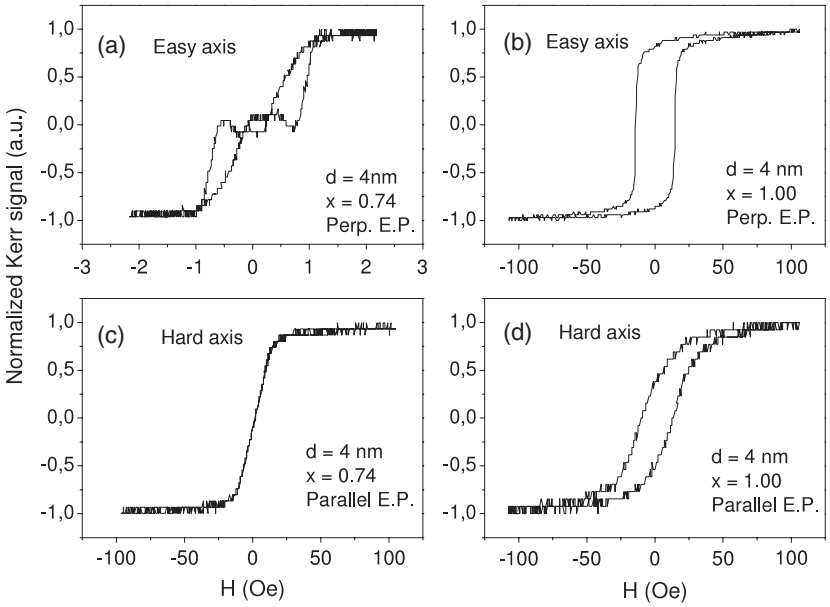

Figure 9. Normalized MOTKE loops of 10 period multilayers. Each period is made of 5 nm of magnetic material and 4 nm Si spacer. Panels (a) and (c) show the easy (magnetic field applied perpendicular to the evaporation plane) and hard axes (magnetic field applied parallel to the evaporation plane) corresponding to a magnetic material having $x = 0.74$ and panels (b) and (d) to the polycrystalline one, $x = 1.00$. Note that panel (a) has a different X axis scale.

a polycrystalline ordering [20, 21]. This structural change leads to very different magnetic behaviours. Figure 5 already shows that amorphous single films develop well-defined in-plane magnetic uniaxial anisotropy. Typical values of the anisotropy fields for 5 nm thick films are around 20 Oe. Also, the easy axis loops have very low coercive fields, only tenths of Oe for $x = 0.74$ and 5 nm thick films. On the contrary, polycrystalline single films with $x = 1.00$ have much higher coercive fields, around 14 Oe for 5 nm films, and smaller anisotropy [8].

Following this trend corresponding to single films, the magnetic behaviour of multilayers prepared by stacking magnetic films of these compositions, either $x = 0.74$ or 1.00, separated with Si, also shows very different features, as can be seen in the MOTKE hysteresis loops of figure 9. Panels 9(a) and (c) correspond, respectively, to the easy and hard axes of the multilayer $(Si^{4\ nm}/Co_{0.74}Si^{5\ nm}_{0.26})_{10}/Si^{4\ nm}$/substrate, that is, the one based on $x = 0.74$ amorphous magnetic material. On the other hand, panels 9(b) and (d) correspond to the easy and hard axes of a similar multilayer, but with $x = 1.00$ instead of $x = 0.74$ for the magnetic layers: $(Si^{4\ nm}/Co^{5\ nm})_{10}/Si^{4\ nm}$/substrate. Figure 9 shows that both easy and hard axis loops change significantly with the magnetic layer composition. The most interesting features appear in the case of the easy axis of the amorphous multilayer, panel 9(a), where the plateau at low magnetic field, with a remanence value close to zero, indicates the formation of an AF state [8]. Interestingly, the magnetic field needed to switch the magnetization from positive ferromagnetic (F) alignment to negative F alignment is very low, only ± 1 Oe, which shows that the coupling strength is very low [8, 9].

On the other hand, the easy axis of the polycrystalline multilayer, panel 9(b), shows no plateau, the remanence is not going down to zero and the coercive field, around 14 Oe, is the same as that of the single 5 nm Co magnetic layers used to build up the multilayer. This is

confirming that, in this case with $x = 1.00$, no AF alignment is formed at remanence. One of the reasons is that the coercive field needed to start the reversal process is much higher than the switching field associated with the coupling, hindering the formation of possible weakly coupled AF states.

Concerning the hard axis, strong differences are also observed between both multilayers, as is evident in panels 9(c) and (d). The $x = 0.74$ multilayer has a closed hard axis loop, mimicking the behaviour of the corresponding single film, indicating a very well-defined in-plane uniaxial magnetic anisotropy, with an anisotropy field to reach saturation of around 20 Oe. As already mentioned, this anisotropy is related to oblique incidence. However, although the oblique incidence is known to be clearly related to the formation of magnetic anisotropies [38], the microscopic details of this effect, interatomic distance anisotropy, mesoscopic islands, or anisotropic roughness, still remain unclear and more studies are needed in order to elucidate them. On the other hand, the case of $x = 1.00$ shows an open hard axis loop typical of polycrystalline films where crystalline anisotropy contributions dominate and average down with the random crystal orientation, so that the formation of a well-defined in-plane anisotropy is hindered.

4. Conclusions

The structural evolution of the Co crystal lattice as Si is introduced in the network has been followed by SXRD in single Co_xSi_{1-x} films with composition ranging between $x = 1.00$ and 0.77. The results show that a continuous process of amorphization is taking place accompanied by a contraction of the unit cell, both in-plane (0.9%) and out-of-plane (0.2%). In-plane SXRD measurements indicate that no significant structural differences in the corresponding peak position and FWHM are detected when measuring along the magnetic easy or hard axes, suggesting that the magnetic anisotropy is not related to asymmetries in the grain size distribution. Magnetic hysteresis loops of single films show an increase of coercive field and a rotation of the magnetic anisotropy as Si concentration is increased in the range $1.00 \leqslant x \leqslant 0.85$. The loops for the multilayers confirm the antiferromagnetic alignment of the magnetic layers when their composition is tuned to be in the amorphous range. Finally, low angle x-ray reflectivity patterns and AES depth profiles have shown that the multilayer stacking is well defined. Furthermore, the asymmetries observed in the AES depth profile signals suggest the formation of intermediate compounds at the broader Co-on-Si interfaces.

Acknowledgments

This work has been supported by the Spanish CICYT under grants FIS2005-07392 and NAN2004-09087. Scientific discussions and technical support from G R Castro and the rest of the ESRF Spline BM25 beamline staff are acknowledged. CQ acknowledges support from the Spanish Government and the European Social Fund through the 'Ramón y Cajal' programme. LZ acknowledges support from Spanish MEC under FPU grant. J I Martín and M Vélez are strongly acknowledged for scientific discussions and critical reading of the manuscript.

References

[1] Toscano S, Briner B, Hopster H and Landlot M 1992 *J. Magn. Magn. Mater.* **114** L6
[2] Fullerton E E, Mattson J E, Lee S R, Sowers C H, Huang Y Y, Felcher G and Bader S D 1992 *J. Magn. Magn. Mater.* **117** L301

[3] de Vries J J, Kohlhepp J, Den Broeder F J A, Coehoorn R, Jungblut R, Reinders A and de Jonge W J M 1997 *Phys. Rev. Lett.* **78** 3023
[4] Gareev R R, Bürgler D E, Buchmeier M, Olligs D, Schreiber R and Grünberg P 2001 *Phys. Rev. Lett.* **87** 157202
[5] Gareev R R, Bürgler D E, Buchmeier M, Schreiber R and Grünberg P 2002 *J. Magn. Magn. Mater.* **240** 235
[6] Croonenborghs B, Almeida F M, L'abbé C, Gareev R R, Rots M, Vantomme A and Meersschaut J 2005 *Phys. Rev.* B **71** 24410
[7] Inomata K, Yusu K and Saito Y 1995 *Phys. Rev. Lett.* **74** 1863
[8] Quirós C, Martín J I, Zárate L, Vélez M and Alameda J M 2005 *Phys. Rev.* B **71** 24423
[9] Zárate L, Quirós C, Vélez M, Rodríguez-Rodríguez G, Martín J I and Alameda J M 2006 *Phys. Rev.* B **74** 14414
[10] Grundy P J, Fallon J M and Blythe H J 2000 *Phys. Rev.* B **62** 9566
[11] Inomata K and Saito Y 1997 *J. Appl. Phys.* **81** 5344
[12] Luciński T, Wandziuk P, Stobiecki F, Andrzejewski B, Kopcewicz M, Hütten A, Reiss G and Szuszkiewicz W 2004 *J. Magn. Magn. Mater.* **282** 248
[13] Yacoub N, Meny C, Bengone O and Panissod P 2006 *Phys. Rev. Lett.* **97** 257206
[14] Gareev R R, Bürgler D E, Buchmeier M, Schreiber R and Grünberg P 2002 *Appl. Phys. Lett.* **81** 1264
[15] Pruneda J M, Robles R, Bouarab S, Ferrer J and Vega A 2001 *Phys. Rev.* B **65** 024440
[16] Enkovaara J, Ayuela A and Nieminen R M 2000 *Phys. Rev.* B **62** 16018
[17] Tugushev V V, Men'shov V N, Nechaev I A and Chulkov E V 2006 *Phys. Rev.* B **74** 184423
[18] Fallon J M, Faunce C A and Grundy P J 2000 *J. Phys.: Condens. Matter* **12** 4075
[19] Fallon J M, Faunce C A and Grundy P J 2000 *J. Appl. Phys.* **88** 2400
[20] Vélez M, Mény C, Valvidares S M, Diaz J, Morales R, Alvarez-Prado L M, Panissod P and Alameda J M 2004 *Eur. Phys. J.* B **41** 517
[21] Díaz J, Morales R, Valvidares S M and Alameda J M 2005 *Phys. Rev.* B **72** 144413
[22] Zilani M A K, Xu H, Wang X S and Wee T S 2006 *Appl. Phys. Lett.* **88** 023121
[23] Zilani M A K, Liu L, Xu H, Feng Y P, Wang X S and Wee A T S 2006 *J. Phys.: Condens. Matter* **18** 6987
[24] Chang H W, Tsay J S, Hung Y C, Yuan F T, Chan W Y, Su W B, Chang C S and Yao Y D 2007 *J. Appl. Phys.* **101** 09D124
[25] Abhaya S, Venugopal Rao G, Kalavathi S, Sastry V S and Amarendra G 2006 *Surf. Sci.* **600** 2762
[26] Joensson C T, Maximov I A, Whitlow H J, Shutthanandan V, Saraf L, McCready D E, Arey B W, Zhang Y and Thevuthasan S 2006 *Nucl. Instrum. Methods Phys. Res.* B **249** 532
[27] Tsay J S, Fu T Y, Lin M H, Yang C S and Yao Y D 2006 *Appl. Phys. Lett.* **88** 102506
[28] Pan J S, Liu R S, Zhang Z, Poon S W, Ong W J and Tok E S 2006 *Surf. Sci.* **600** 1308
[29] Zhang Y, McCready D E, Wang C M, Young J, McKinley M I, Whitlow H J, Razpet A, Possnert G, Zhang T and Wu Y 2006 *Nucl. Instrum. Methods Phys. Res.* B **242** 602
[30] Jaiswal A, Rai S, Tiwari M K, Reddy V R, Lodha G S and Nandedkar R V 2007 *J. Phys.: Condens. Matter* **19** 016001
[31] Cheng S L, Lu S W, Wong S L, Chang C C and Chen H 2007 *J. Cryst. Growth* **300** 473
[32] Dehesa-Martínez C, Blanco-Gutierrez L, Vélez M, Díaz J, Alvarez-Prado L M and Alameda J M 2001 *Phys. Rev.* B **64** 024417
[33] Guinier A 1994 *X-ray Diffraction in Crystals, Imperfect Crystals and Amorphous Bodies* (New York: Dover)
[34] Quirós C, Valvidares S M, Robach O and Ferrer S 2005 *J. Phys.: Condens. Matter* **17** 5551
[35] Fullerton E E, Pearson J, Sowers C H and Bader S D 1993 *Phys. Rev.* B **48** 17432
[36] Bhattacharyya D, Poswal A K, Senthilkumar M, Satyam P V, Balamurugan A K, Tyagi A K and Das N C 2003 *Appl. Surf. Sci.* **214** 259
[37] Ruterana P, Houdy P and Boher P 1990 *J. Appl. Phys.* **68** 1033
[38] Bubendorf J L, Zabrocki S, Garreau G, Hajjar S, Jaafar R, Berling D, Mehdaoui A, Pirri C and Gewinner G 2006 *Europhys. Lett.* **75** 119